Applied Clay Science 289 (2026) 108253

Contents lists available at ScienceDirect

Applied Clay Science

journal homepage: www.elsevier.com/locate/clay

Research paper

Reactive transport modelling of neptunium migration in Opalinus Clay☆

Theresa Hennig [a,*], Madlen Stockmann [b], Claudia Joseph [b], Vinzenz Brendler [c], Tobias Reich [d], Majedeh Sayahi [a], Michael Kühn [a,e]

[a] GFZ Helmholtz Centre for Geosciences, Reactive Fluids und Geomaterials, Telegrafenberg, Potsdam, 14473, Germany
[b] Bundesgesellschaft für Endlagerung mbH (BGE), Eschenstraße 55, Peine, 31224, Germany
[c] Helmholtz-Zentrum Dresden Rossendorf e.V., Institute of Resource Ecology, Bautzner Landstr. 400, Dresden, 01328, Germany
[d] Johannes Gutenberg-Universität Mainz, Department of Chemistry - Nuclear Chemistry, Mainz, 55099, Germany
[e] University of Potsdam, Institute of Geosciences, Karl-Liebknecht-Str. 24-25, Potsdam-Golm, 14476, Germany

ARTICLE INFO

Keywords:
Multi-component diffusion
Sorption
Redox potential
Iron
Illite
Montmorillonite
Pyrite
Np(IV)
Np(V)

ABSTRACT

One-dimensional simulations of Np diffusion through Opalinus Clay (OPA) were conducted. The experimental data were based on two laboratory diffusion experiments. Both experiments used the same setup for two different drill core samples and exhibited differences in the measured Np concentration profiles. Previous studies showed that the Fe(II)-bearing mineral phases in the OPA lead to a partial reduction of the initially used Np(V) to Np(IV). Diffusion and sorption were the governing processes. For the simulation of diffusive transport, both experimentally determined effective diffusion coefficients (single-component) and a species-specific multi-component (MC) diffusion approach were used. Sorption processes were integrated in the reactive transport simulations using surface complexation models for Np(V) and Np(IV) on illite and montmorillonite. Three scenarios were simulated that increased in terms of their geochemical process complexity. Scenario 1 only considered surface complexation of Np(V) on various illite quantities. Redox reactions via pyrite dissolution and oxidation together with surface complexation of Np(IV) and Np(V) on illite and montmorillonite were added to the system in scenario 2. In scenario 3, redox reactions were simulated via Fe associated with the clay minerals. Clay mineral quantity had only a minor effect on the Np distribution in the cores. Instead, the Np(IV)/Np(V) ratio was essential for the migration lengths. The ratio was controlled by the inherent redox potential of the core sample. Consequently, the difference between the experiments could not be attributed to variations in the clay mineral composition of the used core samples, but rather to differences in the initially inherent redox conditions and accessibility of Fe. The simulation results showed that measurements of core mineralogy, composition of boundary solutions as well as determination of Np oxidation states along the concentration profile are essential to capture the entire geochemical picture of future laboratory investigations of redox-active radionuclides.

1. Introduction

Reactive transport simulations enable a process-based description of both radionuclide diffusion and sorption in argillaceous formations. Diffusive transport in nanoporous media depends on the species charge due to electrostatic interactions between the species and the charged clay mineral surfaces. In contrast to anionic species, cationic species are enriched in the diffuse double layer to compensate the negative surface charge resulting in an enhanced diffusion. Neutral species are not subject to electrostatic interactions with the clay mineral surfaces. Theoretically, they are transported through the entire water-saturated pore space (Bourg et al., 2003; Van Loon and Soler, 2003). The multi-component (MC) diffusion approach accounts for species-specific diffusion in nanoporous media by considering coulomb interactions of each species in the pore water solution with the mineral-water interface (Appelo and Wersin, 2007; Appelo et al., 2010; Tournassat and Appelo, 2011; Tournassat and Steefel, 2019). Cation exchange and surface complexation models quantify sorption over a broad range of geochemical conditions while considering the electrical state of the surface, changes in aqueous speciation, and solution composition (Dzombak and Morel, 1990; Stumm et al., 1992; Lützenkirchen, 2006; Zarzycki et al., 2025). Consequently, reactive transport simulations provide advanced approaches to decipher the underlying processes.

☆ This article is part of a Special issue entitled: 'Clay Conf. Hannover 2024' published in Applied Clay Science.

* Corresponding author.
E-mail address: theresa.hennig@gfz.de (T. Hennig).

https://doi.org/10.1016/j.clay.2026.108253
Received 21 April 2025; Received in revised form 2 April 2026; Accepted 21 April 2026
Available online 27 April 2026

^{237}Np is one of the most concerning radionuclides in the context of high-level radioactive waste disposal due to its long half-life (2.14×10^6 a) and relatively high radiotoxicity (Thompson, 1982; Kaszuba and Runde, 1999). Np is a redox-sensitive element and is mainly present in the oxidation states IV and V under environmental conditions (Langmuir, 1997). Np(V), particularly the neptunyl-ion NpO_2^+, has a higher mobility than Np(IV). Np(V) solid phases are more soluble than Np(IV) phases and sorption of aqueous Np(V) species on minerals is less pronounced than of Np(IV) species (Thompson, 1982; Langmuir, 1997; Fröhlich, 2015). Consequently, the migration behaviour of Np is defined by its oxidation state, and thus controlled by the present redox potential of a system (Kaszuba and Runde, 1999).

Np(V) sorption on clay minerals was investigated for decades under varying geochemical conditions, such as pH, partial pressure of carbon dioxide (pCO_2) and oxygen (pO_2), ionic strength, and background electrolyte components (Aksoyoglu et al., 1991; Turner et al., 1998; Schmeide and Bernhard, 2010; Marsac et al., 2015; Banik et al., 2017; Elo et al., 2017; Semenkova et al., 2018; Schacherl et al., 2023). Based on these data, the following main conclusions can be drawn for environmentally relevant conditions ($6 \leq pH \leq 9$). Np sorption on clay minerals depends on (1) pH as it is dominated by surface complexation, (2) pCO_2 as it affects speciation, and (3) the redox potential of the system as it determines the Np oxidation state (Fröhlich, 2015). Nevertheless, some questions about Np migration remain, particularly for natural heterogeneous geological systems such as the Opalinus Clay (OPA).

The geochemistry of the OPA pore water is governed by diagenesis, paleohydrogeology, and water-rock interactions (Wersin et al., 2022). The average OPA mineralogy is given in Table SM1. In nature, the hydrogeochemical system is reducing. The redox potential is assumed to be controlled by the redox couple SO_4^{2-}/HS^-. In geochemical calculations, this is realized by applying an equilibrium between the pore water solution and pyrite together with siderite. In that way, the redox system is indirectly coupled with the carbonate system. However, a dominance or contribution of the Fe(II)/Fe(III) redox couple originating from Fe-containing or clay minerals to the present redox potential cannot be excluded (Wersin et al., 2022). The composition of major cations in the pore water is relatively stable as geochemical perturbations are compensated by cation exchange processes.

Np sorption on and Np diffusion in OPA were investigated in various batch sorption and two diffusion experiments (Wu et al., 2009; Fröhlich et al., 2011, 2012a,b, 2013; Stöbener et al., 2012; Reich et al., 2016; Amayri et al., 2016). In addition to findings from batch sorption experiments with pure clay minerals, Np sorption onto OPA depended also on the presence of Fe(II) in the pore water (Fröhlich et al., 2011, 2012a,b; Stöbener et al., 2012). Although all experiments were performed with Np(V), Np(IV) was also detected, even under aerobic conditions (Fröhlich et al., 2012a). A spatial correlation between Np and Fe was observed by micro-X-ray fluorescence mapping. An Fe-rich spot could be identified as pyrite with micro-X-ray diffraction measurements indicating that reduction was caused by Fe(II)-containing minerals. Np sorption measured in batch experiments was about a factor of four lower compared to diffusion experiments, indicating a partial reduction to Np(IV) in the diffusion process (Wu et al., 2009). In a later diffusion study, results from batch sorption and diffusion experiments were comparable (Fröhlich et al., 2013). The concentration profiles of the two diffusion experiments of Wu et al. (2009) and Fröhlich et al. (2013) differed significantly (Fig. 1). Both studies used the same setup, but different core samples. Therefore, the difference was attributed to mineralogical heterogeneities. With increasing knowledge of Np and OPA chemistry, a quantitative investigation of Np sorption and diffusion processes is still lacking to address the question: What does control Np migration in heterogeneous geological systems?

In the present study, Np migration processes were quantified by taking advantage of reactive transport simulations using the two diffusion experiments in OPA as references. Both experiments were modelled for the first time with process-based simulations. The simulations were set up in different geochemical scenarios including the sorption of Np(V) and Np(IV), redox reactions via the redox couples SO_4^{2-}/HS^- or Fe(II)/Fe(III), and considering species-specific diffusion. This does not only have implications for Np migration in OPA, the results will also give insights into transport processes of other redox-sensitive radionuclides (Ma et al., 2019).

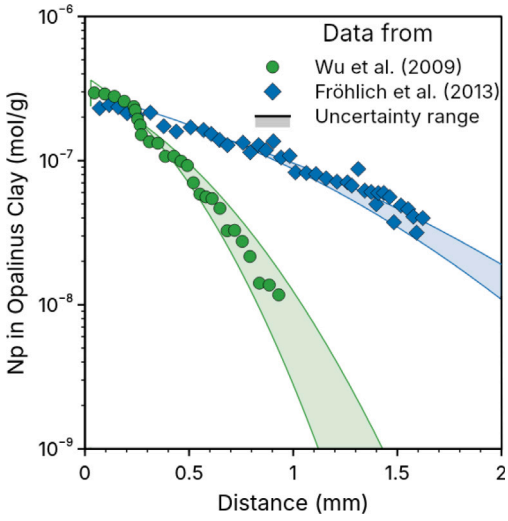

Fig. 1. Concentration profiles of Np in OPA determined by Wu et al. (2009) and Fröhlich et al. (2013). Np was detected up to 1 mm deep in OPA after 37 days (circles) and 1.6 mm after 30 days (diamonds). The uncertainty range was calculated based on the parameter variations determined from the experiments (Table 1).

2. Laboratory experimental setup

The OPA drill cores used in the Np diffusion experiments of Wu et al. (2009) and Fröhlich et al. (2013), hereafter referred to as Wu and Fröhlich, originated from the Mont Terri underground rock laboratory (URL). The exact mineralogy of the used drill cores was not determined, but the core samples differed in their elemental composition, exhibiting a variation of approximately 2 wt.% in Fe content (Table SM2).

The through-diffusion experiments (Van Loon and Soler, 2003) were performed at room temperature. Each cylindrical OPA core sample (diameter: 25.4 mm; length: 11 mm) was sandwiched between two stainless-steel filter plates (diameter: 25.4 mm; length: 1.57 mm) and then mounted in a stainless-steel diffusion cell, which was connected via a peristaltic pump to a source and a receiving reservoir on each side. The reservoirs were filled with artifical OPA pore water that had a pH of 7.6 (Table SM3). Note, the artificial OPA pore water did not contain iron in contrast to *in situ* OPA pore water (Pearson et al., 2003, 2011; Wersin et al., 2022). The transport direction was perpendicular to the clay rock bedding.

Np was only added to the source reservoir as Np(V) with $[^{237}Np]_0$ of 7.4×10^{-6} mol/L for Wu and 8×10^{-6} mol/L for Fröhlich resulting in a concentration gradient across the diffusion cell. The Np concentrations in the source reservoir solutions slightly decreased with time, i.e. about 10% in the case of Wu and even less in the case of Fröhlich. The pH was constant, and the redox conditions were intermittently monitored throughout the diffusion experiments, remaining stable between 0.35 and 0.40 V (Wu et al., 2009; Fröhlich et al., 2013) corresponding to pe values of 5.9–6.8 (for 25°C: $pe = E_H$ (V)/0.059). The receiving reservoir solution was only occasionally replaced. The Np diffusion experiments were terminated after 37 days (Wu) and 30 days (Fröhlich), respectively.

After the diffusion experiments, the Np concentration in the clay was determined. Differences in the measured Np concentration profiles

Table 1
Parameter values for the Np diffusion through OPA obtained by Wu et al. (2009) and Fröhlich et al. (2013): ρ_b bulk density, ϵ_{acc} accessible porosity, D_e effective diffusion coefficient, and K_d distribution coefficient.

Parameter	Unit	BHE-25/10[a]	BLT-14
Data from		Wu et al. (2009)	Fröhlich et al. (2013)
Facies		shaly	lower shaly
ρ_b	kg/m^3	2420 ± 8	2412[b]
ϵ_{acc}	–	0.15 ± 0.01	0.20 ± 0.01
D_e	10^{-11} m^2/s	0.69 ± 0.11	2.30 ± 0.20
K_d	m^3/kg	0.10 ± 0.01	0.046 ± 0.003

[a] The drill core was originally referred to as BAE-25/10 (Wu et al., 2009). This was a typing error.
[b] In Fröhlich et al. (2013), bulk density uncertainty was not given.

were observed (Fig. 1) and accordingly, in the values determined for the effective diffusion coefficient D_e and the distribution coefficient K_d (Table 1). Further details are given in Wu et al. (2009) and Fröhlich et al. (2013).

3. Methods

The diffusion experiments of Wu and Fröhlich were simulated with a one-dimensional reactive transport model. All simulations were conducted in a continuum scale with PHREEQC Version 3 (Parkhurst and Appelo, 2013) using the PSI Thermodynamic Database 2020 (Hummel and Thoenen, 2023). The Specific Ion Interaction Theory (SIT) implemented in the database was used to consider ion-ion interactions. The RedModRphree package was used to create Pourbaix diagrams for Np speciation in artificial OPA pore water (De Lucia and Kühn, 2021). All calculations were carried out for 25°C.

3.1. Integration of sorption processes

Illite and illite/smectite mixed layers, which were assumed to consist of 50% illite and 50% montmorillonite, were considered as OPA mineral components with the highest sorption capacity with respect to radionuclides. Therefore, the 2-Site Protolysis Non-Electrostatic Surface Complexation and Cation Exchange (2SPNE SC/CE) sorption model for illite and montmorillonite (Bradbury and Baeyens, 1997, 2005a) was applied to simulate sorption of Np(IV) and Np(V) on OPA. The thermodynamic database needed to be extended by the sorption data of the Np hydroxo-complexes (Bradbury and Baeyens, 2002, 2006, 2009a,b; Marsac et al., 2015). In addition to surface complexation, cation exchange processes were also taken into account for the main cations in the pore water (Table SM3), Np, and Fe. All surface parameters and reactions can be found in Table SM4.

The Donnan approximation implemented in PHREEQC (Parkhurst and Appelo, 2013) was used to calculate the composition of the diffuse double layer as average assuming a single potential as entity. The thickness of the diffuse double layer was set to 5×10^{-10} m, which was calculated following Wigger and Van Loon (2018) using an ionic strength of 0.4 mol/L (Table SM3).

Clay mineral quantities were varied between 20, 30, and 40 wt.% for illite and 2, 4, and 6 wt.% for montmorillonite since the clay sample-specific values were not known. For the minimum investigated clay mineral quantity, the site capacities for the strong sites on illite were about 4×10^{-7} mol/g and on montmorillonite around 8×10^{-8} mol/g. These capacities exceeded the total amount of Np present in the experiments (Fig. 1), meaning only strong sites needed to be considered for Np sorption in the model. The clay mineral variations were representative for the shaly facies of OPA (Pearson et al., 2003), where both drill cores originated from (Table 1).

3.2. Geochemical scenarios

Three scenarios were simulated that increased in complexity with respect to the geochemical processes taken into account (Table SM5).

(1) The first scenario only considered surface complexation of Np(V) on illite. This means all other mineral and sorption reactions were neglected.

(2) The second scenario considered surface complexation of Np(IV) and Np(V) on illite and montmorillonite as well as cation exchange processes. Mineral reactions with calcite and pyrite were implemented to define pH and redox conditions. Both minerals were assumed to be in equilibrium with the pore water (saturation index SI = 0). The E_H of the source reservoir solution was measured to be between 0.35 to 0.4 V (Section 2), corresponding to pe of 5.9–6.8 and a calculated dissolved O_2 concentration of $<10^{-30}$ mol/L. Common pyrite reaction rates (Williamson and Rimstidt, 1994; Palandri and Kharaka, 2004) did not lead to a reaction under the laboratory conditions (Table SM3) as they are based on O_2, Fe^{3+}, and H^+ as rate controlling species. Instead, a thermodynamic equilibrium approach was applied to investigate the potential role of pyrite as an electron donor pool regardless of these kinetic limitations. Assuming thermodynamic equilibrium for pyrite yielded a dissolved Fe concentration of 10^{-8} mol/L and a pe of −3.8. This calculated state mirrors the reducing *in situ* conditions observed at the Mont Terri URL, providing a realistic bounding scenario for the models. At such a low pe, the overall redox system is predominantly buffered by the SO_4^{2-}/HS^- redox couple. Because of these stable reducing conditions, the presence of Fe(III) is negligible. Consequently, only Fe(II) was considered for Fe surface complexation in scenario 2, and any oxidation of surface-bound Fe to Fe(III) was excluded.

(3) In contrast to scenario 2, in the third scenario redox conditions were controlled via the Fe(II)/Fe(III) redox couple. In unweathered OPA, Fe is mainly present in the form of Fe(II) associated with the clay minerals, i.e., either structural, complexed by surface hydroxyl groups, or bound by ion exchange, followed by Fe(II) in siderite, Fe(III) in clay minerals and Fe(II) in pyrite (Mazurek et al., 2023). Recent studies showed that Fe associated with the clay minerals can be redox-active even at low structural Fe content, and hence can influence the oxidation state of Np (Marsac et al., 2015; Schacherl et al., 2023). The redox reactivity of structural Fe(II) is higher compared to dissolved Fe(II) (Cui and Eriksen, 1996). Electron transfer can occur via both, structural as well as surface-bound Fe (Neumann et al., 2013; Latta et al., 2017). To imitate this electron transfer in the simulations, surface complexation models for Fe including an oxidation reaction were used (Soltermann et al., 2014; Chen et al., 2022) providing electrons for Np(V) reduction (Table SM4). It was assumed that the core samples, and thus the sorption sites, edge as well as planar, had initially reached an equilibrium state of Fe sorption according to the *in situ* pore water composition. As outlined by Chen et al. (2024), Fe(II) in the OPA pore water is in equilibrium with pyrite and siderite defined by the solubility products (K_s) and with the clay minerals controlled by sorption–desorption reactions including ion exchange and surface complexation reactions. This equilibration step was used to introduce Fe into the system and was done prior to the transport simulations.

During the transport simulations, redox conditions were controlled by surface-bound Fe. Mineral reactions with pyrite or siderite were not considered.

Accordingly, the geochemical scenarios differed in terms of the modelled redox system, sorption processes, and clay mineral assemblage. For scenarios 2 and 3, the PHREEQC input files were provided as examples for the Wu model with 20 wt.% illite and 2 wt.% montmorillonite (Table SM5).

3.3. Integration of diffusive transport

Molecular diffusion was assumed to be the only transport process. It was quantified with two approaches, single-component (SC) diffusion using the experimentally determined D_e and MC diffusion to account for species-specific diffusion and electrostatic interaction with the clay mineral surface (Table SM5).

The transport calculations followed Fick's second law and are referred to as SC diffusion in the following. The respective set of values for ρ_b, ϵ_{acc}, and D_e (Table 1) were used to model the measured Np concentration profiles (Fig. 1). Apart from that, the models were the same for both experiments. Porosity was assumed to be constant throughout the modelling domain, therefore diffusion solely depended on the pore water diffusion coefficient D_p (Np), which could be derived via $D_e = \epsilon_{acc} \cdot D_p$. The SC diffusion approach was applied for all scenarios.

The MC diffusion approach implemented in PHREEQC (Appelo and Wersin, 2007; Appelo et al., 2010; Parkhurst and Appelo, 2013) was used to account for species-specific diffusive transport. In this option, D_p was calculated analogue to Archie's law via $D_p = D_w \cdot \epsilon_{acc}^n$. The water diffusion coefficients D_w (m^2/s) for all required species in the pore water are summarized in Table SM6. A D_w of 2.2×10^{-9} m^2/s was used for water (Woolf, 1975; Van Loon et al., 2023). With molecular dynamic simulations for U species, it was shown that D_w did not differ significantly among the aqueous species relevant for the OPA system (Kerisit and Liu, 2010). Therefore, a D_w value of $6.0 \pm 1.0 \times 10^{-10}$ m^2/s as determined by Wu et al. (2009) for NpO_2^+ was chosen for all Np species due to lack of data for the other aqueous Np species present in the system. The empirical exponent n represents a material-specific property of the porous medium and must be determined independently of chemical interactions. Therefore, an inert, non-sorbing tracer is required for its calibration. The value for n was set to 1.629 for Wu and 1.920 for Fröhlich. Through this approach, the D_p of water calculated in PHREEQC matched the experimentally determined D_p of HTO, which had a value of 1.0×10^{-10} m^2/s (Wu et al., 2009; Fröhlich et al., 2013). Due to numerical instabilities, MC diffusion was only used for scenarios 2 and 3.

The boundary conditions referring to the source and receiving reservoir solutions were kept constant (Dirichlet conditions), since the Np concentration decrease in the source reservoir solution was low (<10%) and no Np was detected in the receiving reservoir solutions during the duration of the diffusion experiments (Fig. 1). Spatial resolution was 1.1×10^{-4} m corresponding to 100 cells, whereby grid independence was confirmed by test simulations of finer resolution. Numerical stability was ensured by the Neumann criteria.

4. Results

4.1. Np speciation in artificial Opalinus Clay pore water

The Pourbaix diagram (Fig. 2) was calculated for $[Np]_0 = 1 \times 10^{-9}$ mol/L in artificial OPA pore water for pH from 4 to 10 and E_H from −0.36 V to 0.36 V corresponding to pe values of −6 and 6, respectively. In this way, the range of experimental redox conditions was covered.

Conditions of the source reservoir solution and in OPA *in situ* were highlighted in the diagram as described in Section 2. At pH 7.6, Np(V) dominated the system for pe > 2 and Np(IV) was the dominant oxidation state for pe < 2. The source reservoir solutions were dominated by NpO_2^+ (Fig. 2, Table SM7). Np(IV) species were not present in detectable quantities. Np(IV) and Np(V) would be present in equivalent quantities for a pe of 2. Under *in situ* conditions, $Np(OH)_4(aq)$ would be the main species.

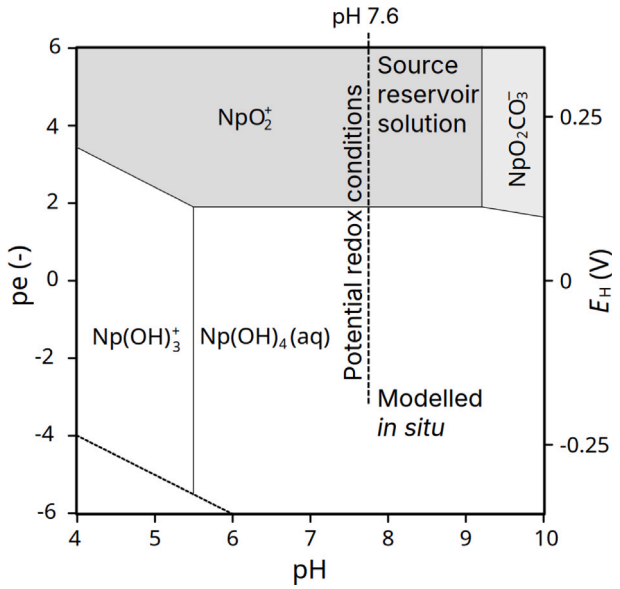

Fig. 2. Pourbaix diagram of Np in artificial OPA pore water with $[Np]_0 = 1 \times 10^{-9}$ mol/L. The pH was constant during the diffusion experiments with a value of 7.6 (dashed line, Table SM3). Np(IV), given in white, and Np(V), shown in grey, were the most stable oxidation states under environmental conditions.

4.2. Simulation of Np migration

For all modelled Np concentration profiles (Figs. 3(a), (b)–5(a), (b)), Np concentrations corresponded to the sum of Np present in the pore water and on the solid phase. Results are shown for the different clay mineral quantities, 20 wt.% illite (dotted lines), 30 wt.% (solid lines), and 40 wt.% illite (dashed lines). Representative modelled pe values (Figs. 4(c) and 5(c)) are shown for the simulations with 20 wt.% illite (dotted lines), as they did not vary significantly for the different clay mineral quantities. Results using the MC diffusion approach are only given for the simulations with 20 wt.% illite (thin dotted line) for a better overview.

4.2.1. Scenario 1 — neglecting redox reactions

Simulations of Np concentration profiles after diffusing into OPA considering only surface complexation of Np(V) on illite are shown in Fig. 3(a), (b).

Modelled concentrations were on the same order of magnitude as the measured concentrations. In the case of Fröhlich (Fig. 3(a)), simulations slightly underestimated measured concentrations at the inlet and overestimated towards the end of the Np front. The fit was improved by increasing the amount of illite in the system. However, the slope of the measured concentrations was steeper towards the end of the Np front than in the simulations. While the simulations of scenario 1, considering only sorption of Np(V) on illite, did not fully reproduce the overall slope of the measured profile, they provided a reasonable approximation of the experimental Np concentrations for Fröhlich. In contrast to Fröhlich, the Wu experiment could not be simulated by this approach, independently of the illite quantity. Scenario 1 was a relatively sufficient approach for the Fröhlich experimental data, whereas this was not the case for the Wu data set. Changing the clay mineral quantity had only a minor effect on the results.

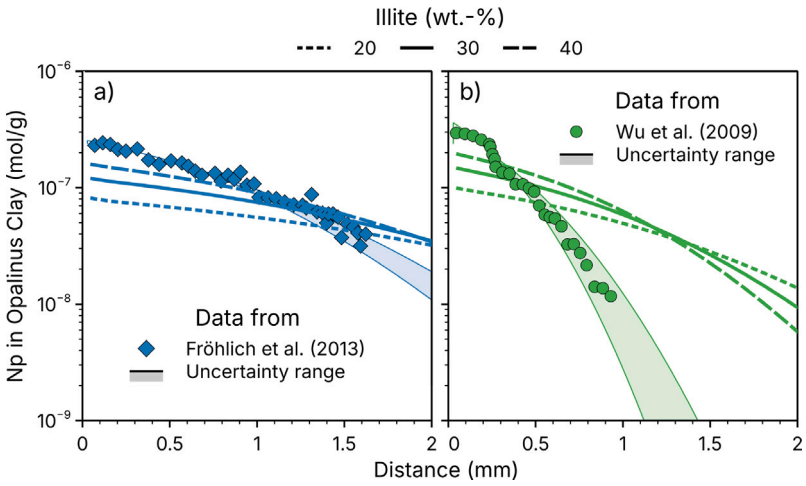

Fig. 3. Scenario 1 — Experimental vs. simulated Np concentration profiles for the (a) Fröhlich (diamonds) and (b) Wu experiment (circles). The simulations considered only surface complexation of Np(V) on illite (Table SM5).

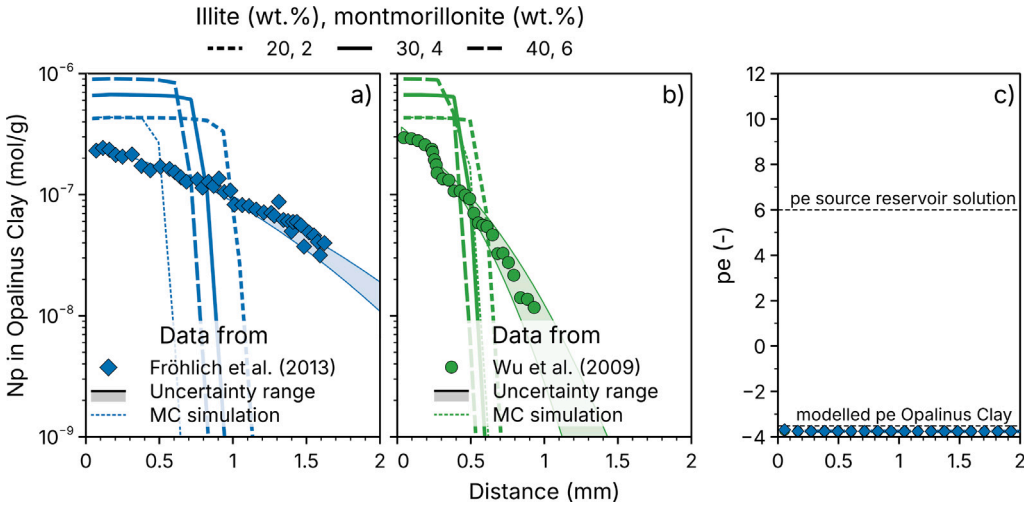

Fig. 4. Scenario 2 — Experimental vs. simulated Np concentration profiles for the (a) Fröhlich (diamonds) and (b) Wu experiment (circles). The geochemical processes included in scenario 2 are listed in Table SM5. (c) Modelled pe values of Fröhlich (dotted line with diamonds) and Wu (dotted line with circles) as a function of diffusion distance. MC = multi-component.

4.2.2. Scenario 2 — redox control via the SO_4^{2-}/HS^- couple

Simulated Np concentration profiles of scenario 2 are shown in Fig. 4(a), (b). Modelled pe values were around −3.8 (Fig. 4(c)) for both Fröhlich (dashed line with diamonds) and Wu (dashed line with circles), which corresponded to *in situ* redox conditions of the OPA formation, indicating that Np(IV) was the dominant oxidation state (Fig. 2).

The simulated curves showed that sorption was overestimated when surface complexation of Np(IV) was considered. Lower clay mineral quantities were associated with lower Np concentrations at the inlet, and thus migration distances into the core sample increased. For all simulations, sorption on montmorillonite accounted for ~10% of the total sorbed Np (not shown). Neither the data of Fröhlich (Fig. 4(a)) nor the data of Wu (Fig. 4(b)) could be resembled by the simulations of scenario 2. However, the modelled steep slope was more consistent with the profile of Wu. For both experiments, results using MC diffusion were similar and migration distances decreased, particularly in the case of Fröhlich.

4.2.3. Scenario 3 — redox control via the Fe(II)/Fe(III) couple

Results for scenario 3 are shown in Figs. 5(a), (b). Initially, the pe corresponded to conditions *in situ* of the OPA formation. As soon as Np(V) diffusion started, the pe increased with time up to a value of 2 at the inlet and decreased along the core sample towards the receiving reservoir as can be seen in Fig. 5(c). In the pore water (not shown), Np was present as a mixture of Np(IV) and Np(V), whereby the fraction of Np(IV) increased along the core sample. The sorbed fraction of Np predominantly consisted of Np(IV). Sorption on montmorillonite was <5% of the total sorbed Np. Sorption was almost 100% (not shown) so that the system was dominated by Np(IV).

The experimental Np concentration profile of Fröhlich (Fig. 5(a)) could be simulated by the model with 20 wt.% illite and 2 wt.% montmorillonite using the experimentally determined D_e (Fig. 1; SC approach). With the MC option (thin dotted line), the modelled Np concentration profile decrease was too sharp. In contrast, the Wu MC diffusion model (thin dotted line, Fig. 5(b)) improved the match with the data, particularly towards the end of the diffusion profile. However,

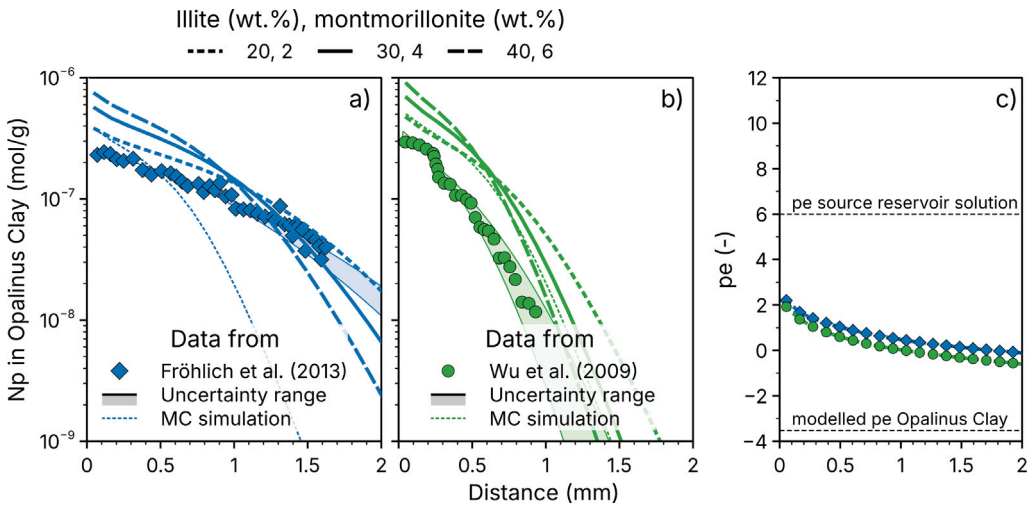

Fig. 5. Scenario 3 — Experimental vs. simulated Np concentration profile for the (a) Fröhlich (diamonds) and (b) Wu experiments (circles). They were modelled assuming a redox control via Fe(II)/Fe(III) redox couple associated with the clay minerals (Table SM5). (c) Modelled pe values of Fröhlich (dotted line with diamonds) and Wu (dotted line with circles) as a function of diffusion distance. MC = multi-component.

modelled Np concentrations at the inlet and centre of the profile were still too high compared to the measurements. In case of Wu (Fig. 5(b)), Np concentrations were overestimated using the SC approach (Table 1).

5. Discussion

5.1. Effect of clay mineral quantity

The effect of different clay mineral quantities on the modelled concentration curves was shown in scenario 1 (Fig. 3(a), (b)). A redox control, that could have affected the modelled concentration profile, was not included. Doubling the illite quantity from 20 wt.% to 40 wt.% had only a minor effect on the modelled concentration profile. This was also the case for scenarios 2 and 3 (Figs. 4(a), (b) and 5(a), (b)). Nevertheless, the geochemically simple scenario 1 indicated that the Fröhlich system was dominated by migrating Np(V). Montmorillonite accounted for only ~10% of the total Np sorption in the case of scenario 2 and even less in the case of scenario 3. Hence, Np sorption could be modelled considering only illite. In general, changing the illite quantity had only a minor effect on the modelled Np concentration profiles, illustrating that the difference between the diffusion experiments of Wu and Fröhlich could not solely be attributed to variations in the clay mineral composition of the used core samples.

5.2. Effect of redox couple

Assuming pyrite equilibrium with the pore water (SI = 0, scenario 2), led to the predominance of Np(IV). The initially simulated pe of the core sample was about −3.8 (Fig. 4(c)), i.e., *in situ*, and thus corresponded to the Np(IV) predominance field (Fig. 2). However, the source reservoir solution had a pe of 6 meaning Np entered the system as Np(V), but would not be thermodynamically stable. This resulted in a sharp E_H gradient across the reservoir solution-rock interface as also outlined by Kaplan et al. (2024). As soon as Np(V) entered the system, pyrite dissolved and oxidized to Fe(III) and SO_4^{2-}, providing electrons for Np(V) reduction to Np(IV). Np(IV) has a higher affinity to form complexes with the hydroxyl groups on the surface edge sites of illite and montmorillonite than Np(V), and is therefore less mobile (Bradbury and Baeyens, 2005b; Marsac et al., 2015). This was reflected in the calculated concentration profiles (Fig. 4(a), (b)), which dropped abruptly in contrast to the simulations of scenario 1 (Fig. 3(a), (b)). However, the modelled Np concentrations at the inlet were too high and overall migration distances too short compared to the experimental data. In conclusion, the assumption of pyrite dissolution and oxidation occurring at thermodynamic equilibrium, meaning the predominance of the SO_4^{2-}/HS^- redox couple, was not an appropriate approach to describe the experimental observations due to the sensitivity of the Np system to the redox state.

Redox processes via Fe associated with the clay minerals is another conceptual modelling approach, which was applied in scenario 3. Similar to scenario 2, pe values and aqueous Fe concentrations corresponded to *in situ* conditions. When Np(V) diffused into the core sample, Fe(II) on the mineral surface was oxidized to Fe(III) and Np(V) was reduced to Np(IV). However, the half-reaction of Fe(II) oxidation on the clay mineral surface provided only one electron (Table SM4) in contrast to the oxidation of pyrite. Hence, not all Np(V) entering the system was reduced leading to a mixture of aqueous Np(V) and Np(IV) species and an enhanced simulated pe. This caused some differences in the concentration profiles (Fig. 4 and 5). Overall, Np(IV) was the dominant oxidation state and most of the Np was sorbed. Marsac et al. (2015) showed that Np(IV) surface species are thermodynamically favoured even within the predominance field of Np(V) aqueous species. This could be related to a surface-mediated reduction process by oxidation of structural Fe or adsorbed Fe. Many studies showed that Fe associated with the clay minerals is redox-active (Hofstetter et al., 2003; Schaefer et al., 2011; Gorski et al., 2012, 2013; Soltermann et al., 2014; Latta et al., 2017; Chen et al., 2022). For instance, Glaus et al. (2008) observed that reduction of iodate to iodide occurred as soon as it was in contact with OPA, which was also related to Fe(II)-bearing mineral phases. With respect to the total Fe pool in OPA, the fraction of Fe associated with clay minerals is larger than that associated with pyrite and siderite (Mazurek et al., 2023). In conclusion, clay minerals play an important role for redox processes and seem to be the main electron donor for Np(V) reduction in OPA.

Although the redox control in OPA seems to be related to Fe(II) associated with clay minerals, it was observed that Np is allocated with pyrite (Fröhlich et al., 2012a). In agreement with this observation, Hoving et al. (2017) showed for Boom Clay that its redox response is a combination of Fe associated with the clay minerals, representing a highly reactive, spatially dispersed electron donor pool, and pyrite as localized redox-active phase with slower kinetics. In addition, it needs to be taken into account that different fractions of pyrite, as observed for marine sediments, react on different time scales depending on their morphology, framboidal or euhedral (Morse, 1991). This could not be reproduced with the chosen approach of thermodynamic equilibrium forcing the system to low redox conditions.

Thus, a kinetic approach might be more appropriate to accurately capture the geochemical system. However, pyrite reaction rates have so far been described as a function of O_2 intrusion as well as H^+ and Fe^{3+} concentrations (Williamson and Rimstidt, 1994; Palandri and Kharaka, 2004). The measured E_H of the source reservoir solution remained within a stable range of 0.35–0.4 V throughout the Np diffusion experiment (Wu et al., 2009; Fröhlich et al., 2013) corresponding to a calculated dissolved O_2 concentration of less than 10^{-30} mol/L (Table SM3). Thus, a rate law formulation using other rate controlling species, such as Np, need to be developed and tested in future works.

5.3. Effect of species-specific diffusion

Np migration lengths were shorter when the MC diffusion approach was used than in simulations using the SC approach. This could be explained by differences in the D_p values for Np. The D_p used in the MC simulations was calculated to be 2.7×10^{-11} m^2/s in both the Fröhlich and Wu cases. However, the SC approach D_p (D_e/ϵ_{acc}, Table 1) were about a factor of 4 higher in the case of Fröhlich ($D_p = 11.5 \times 10^{-11}$ m^2/s) and a factor of almost 2 higher in the case of Wu ($D_p = 4.6 \times 10^{-11}$ m^2/s). This explains why the difference in migration lengths between SC and MC diffusion simulations was more pronounced for Fröhlich. A smaller D_p was used with the MC option resulting in shorter migration distances.

The oxidation state governs sorption and diffusion behaviour. The fit between model and experimental data improved using the MC option in the case of Wu, but not in the case of Fröhlich. In both scenarios, 2 (Figs. 4(a), (b)) and 3 (Figs. 5(a), (b)), the modelled system was dominated by Np(IV), which was mainly present as neutral complex $Np(OH)_4(aq)$ (Fig. 2) and in minor quantities as anionic complex $Np(OH)_2(CO_3)_2^{2-}$ (Table SM7). Anionic species are excluded from the diffuse double layer. Accounting for species-specific diffusion with the MC option means that the accessible pore space of the anionic aqueous Np(IV) species was diminished resulting in lower D_p values and overall shorter migration distances. Thus, the migration behaviour of Np depends on the pe defining the specific aqueous Np speciation. Depending on their charge, the species are distributed between pore water and diffuse double layer resulting in a different diffusion behaviour. Consequently, although the same D_w was used for all Np species, the migration behaviour differed. This aspect is also reflected in the experimentally determined D_e (Table 1). The D_e value of Fröhlich was higher than the value of Wu indicating a higher proportion of Np(V) in the Fröhlich system. The modelled system was dominated by Np(IV), what is more in line with the Wu concentration profile. Fröhlich could only be modelled using the experimentally D_e. MC diffusion is required to quantify Np migration as the predominance of Np(IV) results in higher sorption and lower diffusion (Wu) compared to Np(V) characterized by lower sorption and enhanced diffusion (Fröhlich).

The difference between the experiments cannot solely be related to mineralogical heterogeneities. Both the experiments of Wu and Fröhlich were performed under constant and monitored redox conditions using the same setup, but the core samples were processed differently. The Fröhlich sample was aerobic (Fröhlich et al., 2013), whereas the Wu sample was cut under inert gas (Wu et al., 2009). Fröhlich et al. (2012a) showed that samples handled under anaerobic conditions contained a significantly higher amount of Np(IV) compared to aerobic samples. It can be postulated, that the inherent pe of the core sample could have been lower in the case of Wu forcing Np(V) reduction, and thus a stronger sorption and lower diffusivity due to a higher Np(IV) fraction. In addition, the Fe content of the Wu core sample was roughly 2 wt.% higher than in the Fröhlich sample representing a larger electron donor pool (Table SM2). In contrast, the Fröhlich profile could be approximated including only sorption of Np(V) in the simulations. This together with the higher D_e indicated that the proportion of Np(V) was higher in the Fröhlich sample than in the Wu sample. It can be concluded that the difference in the measured Np concentration profiles was due to differences in the initial redox conditions between the core samples, caused either by the processing of the core samples or by differences in the electron donor pool due to mineralogical heterogeneities.

6. Conclusions

The relevant processes for the quantification of Np migration through Opalinus Clay (OPA) were identified by means of reactive transport simulations using surface complexation models and multi-component (MC) diffusion. Data of two diffusion studies with the same experimental setup, but different core samples and Np concentration profiles were investigated. Geochemical processes were varied to assess their impact on the modelled Np concentration profiles in scenarios.

The following recommendations for Np migration through OPA were concluded based on the simulations: Np migration (1) should be modelled considering species-specific sorption and MC diffusion of both Np(IV) and Np(V), (2) is mainly governed by the redox conditions of the core sample as this determines the fractions of Np(IV) and Np(V) and with that the migration behaviour in the system. (3) The clay mineral quantity has only a minor impact.

Some implications for future experiments with redox-active radionuclides can be derived. (a) The mineralogical composition of the used core samples was not determined. For this reason, the clay mineral quantities were varied within plausible ranges, and thus were used as a free or fitting parameter. Clay mineralogical measurements of the used core samples would constrain the system further, but were not the decisive factor. Knowledge about the mineralogy of redox-active phases is essential to make reliable assumptions. (b) Redox and pH conditions were monitored for the source reservoir solution, but not for the receiving reservoir solution. Regular measurements of the receiving reservoir solution composition would help to identify possible changes due to exchange or redox reactions, e.g., of Fe. (c) Not only the total Np concentration profile is essential for the evaluation of the experiments, but also the Np(IV) and Np(V) distribution is crucial to get the entire geochemical picture. The processing of the core sample seems to play an important role. Accordingly, *in situ* conditions should be maintained during processing wherever possible. In contrast, "atmospheric" conditions in the laboratory are not a problem, if the reservoir solutions are well monitored. Future diffusion experiments with redox-active radionuclides should include measurements of the core mineralogy, receiving reservoir solution composition as well as determination of oxidation states along the concentration profile.

CRediT authorship contribution statement

Theresa Hennig: Writing – original draft, Visualization, Software, Methodology, Investigation, Formal analysis, Data curation, Conceptualization. **Madlen Stockmann:** Writing – review & editing, Methodology, Investigation, Conceptualization. **Claudia Joseph:** Writing – review & editing, Methodology, Investigation, Conceptualization. **Vinzenz Brendler:** Writing – review & editing, Methodology, Investigation, Conceptualization. **Tobias Reich:** Writing – review & editing, Methodology, Investigation, Conceptualization. **Majedeh Sayahi:** Validation, Data curation. **Michael Kühn:** Writing – review & editing, Supervision, Methodology, Investigation, Funding acquisition, Conceptualization.

Financial support

This research did not receive any specific grant from funding agencies in the public, commercial, or not-for-profit sectors.

Declaration of competing interest

The authors declare, that they have no known competing financial interests or personal relationships, that could have appeared to influence the work reported in this paper.

Appendix A. Supplementary data

Supplementary material related to this article can be found online at https://doi.org/10.1016/j.clay.2026.108253.

References

Aksoyoglu, S., Burkart, W., Goerlich, W., 1991. Sorption of neptunium on clays. J. Radioanal. Nucl. Chem. Artic. 149, 119–122. http://dx.doi.org/10.1007/BF02053719.

Amayri, S., Fröhlich, D.R., Kaplan, U., Trautmann, N., Reich, T., 2016. Distribution coefficients for the sorption of Th, U, Np, Pu, and Am on Opalinus Clay. Radiochim. Acta 104, 33–40. http://dx.doi.org/10.1515/ract-2015-2409.

Appelo, C.A.J., Van Loon, L.R., Wersin, P., 2010. Multi-component diffusion of a suite of tracers (HTO, Cl, Br, I, Na, Sr, Cs) in a single sample of Opalinus Clay. Geochim. Cosmochim. Acta 74, 1201–1219. http://dx.doi.org/10.1016/j.gca.2009.11.013.

Appelo, C.A.J., Wersin, P., 2007. Multi-component diffusion in clay systems with application to the diffusion of tritium, iodide, and sodium in Opalinus Clay. Environ. Sci. Technol. 41, 5002–5007. http://dx.doi.org/10.1021/es0629256.

Banik, N.L., Marsac, R., Lützenkirchen, J., Marquardt, C.M., Dardenne, K., Rothe, J., Bender, K., Geckeis, H., 2017. Neptunium sorption and redox speciation at the illite surface under highly saline conditions. Geochim. Cosmochim. Acta 215, 421–431. http://dx.doi.org/10.1016/j.gca.2017.08.008.

Bourg, I.C., Bourg, A.C.M., Sposito, G., 2003. Diffusion and adsorption in compacted bentonite: A critical review. J. Contam. Hydrol. 61, 293–302. http://dx.doi.org/10.1016/S0169-7722(02)00128-6.

Bradbury, M.H., Baeyens, B., 1997. A mechanistic description of Ni and Zn on Na-montmorillonite: Part II: Modelling. J. Contam. Hydrol. 27, 223–248.

Bradbury, M.H., Baeyens, B., 2002. Pore Water Chemistry in Compacted Re-Saturated MX-80 Bentonite: Physico-Chemical Characterisation and Geochemical Modelling. PSI-Report 02-10, Paul Scherer Institut (PSI), Villigen, Switzerland.

Bradbury, M.H., Baeyens, B., 2005a. Experimental and modelling investigations on Na-illite: Acid-base behaviour and the sorption of strontium, nickel, europium and uranyl. Nagra Technical Report TR 04-02, Nagra, Wettingen, Switzerland.

Bradbury, M.H., Baeyens, B., 2005b. Modelling the sorption of Mn(II), Co(II), Ni(II), Zn(II), Cd(II), Eu(III), Am(III), Sn(IV), Th(IV), Np(V) and U(VI) on montmorillonite: Linear free energy relationships and estimates of surface binding constants for some selected heavy metals and actinide. Geochim. Cosmochim. Acta 69, 875–892. http://dx.doi.org/10.1016/j.gca.2004.07.020.

Bradbury, M., Baeyens, B., 2006. Modelling sorption data for the actinides Am(III), Np(V) and Pa(V) on montmorillonite. Radiochim. Acta 94, 619–625. http://dx.doi.org/10.1524/ract.2006.94.9.619.

Bradbury, M.H., Baeyens, B., 2009a. Sorption modelling on illite Part I: Titration measurements and the sorption of Ni, Co, Eu and Sn. Geochim. Cosmochim. Acta 73, 990–1003. http://dx.doi.org/10.1016/j.gca.2008.11.017.

Bradbury, M.H., Baeyens, B., 2009b. Sorption modelling on illite. Part II: Actinide sorption and linear free energy relationships. Geochim. Cosmochim. Acta 73, 1004–1013. http://dx.doi.org/10.1016/j.gca.2008.11.016.

Chen, P., Van Loon, L.R., Koch, S., Alt-Epping, P., Reich, T., Churakov, S.V., 2024. Reactive transport of diffusive mobility and retention of TcO_4^- in Opalinus Clay. Appl. Clay Sci. 251, 107327. http://dx.doi.org/10.1016/j.clay.2024.107327.

Chen, P., Van Loon, L.R., Marques Fernandes, M., Churakov, S., 2022. Sorption mechanism of Fe(II) on illite: Sorption and modelling. Appl. Geochem. 143, 105389. http://dx.doi.org/10.1016/j.apgeochem.2022.105389.

Cui, D., Eriksen, T.E., 1996. Reduction of Tc(VII) and Np(V) in Solution by Ferrous Iron - A Laboratory Study of Homogeneous and Heterogeneous Redox Processes. Technical Report TR 96-03. SKB, Royal Institute of Technology, Stockholm, Sweden.

De Lucia, M., Kühn, M., 2021. Geochemical and reactive transport modelling in R with the RedModRphree package. Adv. Geosci. 56, 33–43. http://dx.doi.org/10.5194/adgeo-56-33-2021.

Dzombak, D.A., Morel, F.M.M., 1990. Surface Complexation : Hydrous Ferric Oxide. Wiley, New York.

Elo, O., Müller, K., Ikeda-Ohno, A., Bok, F., Scheinost, A.C., Hölttä, P., Huittinen, N., 2017. Batch sorption and spectroscopic speciation studies of neptunium uptake by montmorillonite and corundum. Geochim. Cosmochim. Acta 198, 168–181. http://dx.doi.org/10.1016/j.gca.2016.10.040.

Fröhlich, D.R., 2015. Sorption of neptunium on clays and clay minerals – A review. Clays Clay Miner. 63, 262–276. http://dx.doi.org/10.1346/CCMN.2015.0630402.

Fröhlich, D.R., Amayri, S., Drebert, J., Grolimund, D., Huth, J., Kaplan, U., Krause, J., Reich, T., 2012a. Speciation of Np(V) uptake by Opalinus Clay using synchrotron microbeam techniques. Anal. Bioanal. Chem. 404, 2151–2162. http://dx.doi.org/10.1007/s00216-012-6290-2.

Fröhlich, D.R., Amayri, S., Drebert, J., Reich, T., 2011. Sorption of neptunium(V) on Opalinus Clay under aerobic/anaerobic conditions. Radiochim. Acta 99, 71–77. http://dx.doi.org/10.1524/ract.2011.1798.

Fröhlich, D.R., Amayri, S., Drebert, J., Reich, T., 2012b. Influence of temperature and background electrolyte on the sorption of neptunium(V) on Opalinus Clay. Appl. Clay Sci. 69, 43–49. http://dx.doi.org/10.1016/j.clay.2012.08.004.

Fröhlich, D.R., Amayri, S., Drebert, J., Reich, T., 2013. Influence of humic acid on neptunium(V) sorption and diffusion in Opalinus Clay. Radiochim. Acta 101, 553–560. http://dx.doi.org/10.1524/ract.2013.2059.

Glaus, M.A., Müller, W., Van Loon, L.R., 2008. Diffusion of iodide and iodate through Opalinus Clay: Monitoring of the redox state using an anion chromatographic technique. Appl. Geochem. 23, 3612–3619. http://dx.doi.org/10.1016/j.apgeochem.2008.08.013.

Gorski, C.A., Aeschbacher, M., Soltermann, D., Voegelin, A., Baeyens, B., Marques Fernandes, M., Hofstetter, T.B., Sander, M., 2012. Redox properties of structural Fe in clay minerals. 1. Electrochemical quantification of electron-donating and -accepting capacities of smectites. Environ. Sci. Technol. 46, 9360–9368. http://dx.doi.org/10.1021/es3020138.

Gorski, C.A., Klüpfel, L.E., Voegelin, A., Sander, M., Hofstetter, T.B., 2013. Redox properties of structural Fe in clay minerals: 3. Relationships between smectite redox and structural properties. Environ. Sci. Technol. 47, 13477–13485. http://dx.doi.org/10.1021/es403824x.

Hofstetter, T.B., Schwarzenbach, R.P., Haderlein, S.B., 2003. Reactivity of Fe(II) species associated with clay minerals. Environ. Sci. Technol. 37, 519–528. http://dx.doi.org/10.1021/es025955r.

Hoving, A.L., Sander, M., Bruggeman, C., Behrends, T., 2017. Redox properties of clay-rich sediments as assessed by mediated electrochemical analysis: Separating pyrite, siderite and structural Fe in clay minerals. Chem. Geol. 457, 149–161. http://dx.doi.org/10.1016/j.chemgeo.2017.03.022.

Hummel, W., Thoenen, T., 2023. The PSI Chemical Thermodynamic Database 2020. Nagra Technical Report TR 21-03, Nagra, Wettingen, Switzerland.

Kaplan, U., Amayri, S., Drebert, J., Grolimund, D., Reich, T., 2024. Plutonium mobility and reactivity in a heterogeneous clay rock barrier accented by synchrotron-based microscopic chemical imaging. Sci. Rep. 14, 1–11. http://dx.doi.org/10.1038/s41598-024-53189-8.

Kaszuba, J.P., Runde, W.H., 1999. The aqueous geochemistry of neptunium: Dynamic control of soluble concentrations with applications to nuclear waste disposal. Environ. Sci. Technol. 33, 4427–4433. http://dx.doi.org/10.1021/es990470x.

Kerisit, S., Liu, C., 2010. Molecular simulation of the diffusion of uranyl carbonate species in aqueous solution. Geochim. Cosmochim. Acta 74, 4937–4952. http://dx.doi.org/10.1016/j.gca.2010.06.007.

Langmuir, D., 1997. Aqueous Environmental Geochemistry. Prentice Hall, Upper Saddle River, N.J.

Latta, D.E., Neumann, A., Premaratne, W.A., Scherer, M.M., 2017. Fe(II)-Fe(III) electron transfer in a clay mineral with low fe content. ACS Earth Space Chem. 1, 197–208. http://dx.doi.org/10.1021/acsearthspacechem.7b00013.

Lützenkirchen, J., 2006. Surface Complexation Modelling. In: Interface Science and Technology, Vol. 11, Academic Press, Amsterdam London.

Ma, B., Charlet, L., Fernandez-Martinez, A., Kang, M., Madé, B., 2019. A review of the retention mechanisms of redox-sensitive radionuclides in multi-barrier systems. Appl. Geochem. 100, 414–431. http://dx.doi.org/10.1016/j.apgeochem.2018.12.001.

Marsac, R., Banik, N.L., Lützenkirchen, J., Marquardt, C.M., Dardenne, K., Schild, D., Rothe, J., Diascorn, A., Kupcik, T., Schäfer, Th., Geckeis, H., 2015. Neptunium redox speciation at the illite surface. Geochim. Cosmochim. Acta 152, 39–51. http://dx.doi.org/10.1016/j.gca.2014.12.021.

Mazurek, M., Wersin, P., Hadi, J., Grenèche, J.M., Prinpreecha, N., Traber, D., 2023. Geochemistry and palaeo-hydrogeology of the weathered zone in the Opalinus Clay. Appl. Clay Sci. 232, http://dx.doi.org/10.1016/j.clay.2022.106793.

Morse, J.W., 1991. Oxidation kinetics of sedimentary pyrite in seawater. Geochim. Cosmochim. Acta 55, 3665–3667. http://dx.doi.org/10.1016/0016-7037(91)90064-C.

Neumann, A., Olson, T.L., Scherer, M.M., 2013. Spectroscopic evidence for Fe(II)-Fe(III) electron transfer at clay mineral edge and basal sites. Environ. Sci. Technol. 47, 6969–6977. http://dx.doi.org/10.1021/es304744v.

Palandri, J., Kharaka, Y.K., 2004. A compilation of rate parameters of water-mineral interaction kinetics for application to geochemical modelling. Open File Report 2004-1068, U.S. Geological Survey, Menlo Park, California.

Parkhurst, D.L., Appelo, C.A.J., 2013. Description of input and examples for PHREEQC Version 3 – A computer program for speciation, batch-reaction, one-dimensional transport, and inverse geochemical calculations. In: U.S. Geological Survey (USGS) Techniques and Methods. USGS, p. 497, Book 6, Chap. A43.

Pearson, F.J., Arcos, D., Bath, A., Boisson, J.Y., Fernández, A.M., Gäbler, H.E., Gaucher, E.C., Gautschi, A., Griffault, L., Hernán, P., Waber, H.N., 2003. Mont Terri Project – Geochemistry of water in the Opalinus Clay formation at the Mont Terri rock laboratory. Reports of the FOWG 5, Federal Office for Water and Geology, FOWG, Bern, Switzerland.

Pearson, F.J., Tournassat, C., Gaucher, E.C., 2011. Biogeochemical processes in a clay formation in situ experiment: Part E - Equilibrium controls on chemistry of pore water from the Opalinus Clay, Mont Terri underground research laboratory, Switzerland. Appl. Geochem. 26, 990–1008. http://dx.doi.org/10.1016/j.apgeochem.2011.03.008.

Reich, T., Amayri, S., Börner, P.J.B., Drebert, J., Fröhlich, D.R., Grolimund, D., Kaplan, U., 2016. Speciation of neptunium during sorption and diffusion in natural clay. J. Phys.: Conf. Ser. 712, http://dx.doi.org/10.1088/1742-6596/712/1/012081.

Schacherl, B., Joseph, C., Beck, A., Lavrova, P., Schnurr, A., Dardenne, K., Geyer, F., Cherkezova-Zheleva, Z., Göttlicher, J., Geckeis, H., Vitova, T., 2023. Np(V) retention at the Illite du Puy surface. Environ. Sci. Technol. 57, 11185–11194. http://dx.doi.org/10.1021/acs.est.2c09356.

Schaefer, M.V., Gorski, C.A., Scherer, M.M., 2011. Spectroscopic evidence for interfacial Fe(II)-Fe(III) electron transfer in a clay mineral. Environ. Sci. Technol. 45, 540–545. http://dx.doi.org/10.1021/es102560m.

Schmeide, K., Bernhard, G., 2010. Sorption of Np(V) and Np(IV) onto kaolinite: Effects of pH, ionic strength, carbonate and humic acid. Appl. Geochem. 25, 1238–1247. http://dx.doi.org/10.1016/j.apgeochem.2010.05.008.

Semenkova, A.S., Romanchuk, A.Y., Krupskaya, V.V., Pokidko, B.V., Dorzhieva, O.V., Sobolev, A.V., Presnyakov, I.A., Verma, P.K., Mohapatra, P.K., Kalmykov, S.N., 2018. Np(V) uptake by various clays. Appl. Geochem. 92, 1–8. http://dx.doi.org/10.1016/j.apgeochem.2018.02.006.

Soltermann, D., Baeyens, B., Bradbury, M.H., Marques Fernandes, M., 2014. Fe(II) uptake on natural montmorillonites. II. Surface complexation. Environ. Sci. Technol. 48, 8698–8705. http://dx.doi.org/10.1021/es501902f.

Stöbener, N., Amayri, S., Gehl, A., Kaplan, U., Malecha, K., Reich, T., 2012. Sensitive redox speciation of neptunium by CE-ICP-MS. Anal. Bioanal. Chem. 404, 2143–2150. http://dx.doi.org/10.1007/s00216-012-6423-7.

Stumm, W., Sigg, L., Sulzberger, B., 1992. Chemistry of the Solid-Water Interface: Processes at the Mineral-Water and Particle-Water Interface in Natural Systems. J. Wiley & Sons, New York, United States of America.

Thompson, R.C., 1982. Neptunium: The neglected actinide: A review of the biological and environmental literature. Radiat. Res. 90, 1. http://dx.doi.org/10.2307/3575792, arXiv:3575792.

Tournassat, C., Appelo, C.A.J., 2011. Modelling approaches for anion-exclusion in compacted Na-bentonite. Geochim. Cosmochim. Acta 75, 3698–3710. http://dx.doi.org/10.1016/j.gca.2011.04.001.

Tournassat, C., Steefel, C.I., 2019. Reactive transport of coupled processes in nanoporous media. Rev. Miner. Geochem. 85, 75–109. http://dx.doi.org/10.2138/rmg.2019.85.4.

Turner, D.R., Pabalan, R.T., Bertetti, F.P., 1998. Neptunium(V) sorption on montmorillonite: An experimental and surface complexation study. Clays Clay Miner. 46, 256–269. http://dx.doi.org/10.1346/CCMN.1998.0460305.

Van Loon, L.R., Bunic, P., Frick, S., Glaus, M.A., Wüst, R.A.J., 2023. Diffusion of HTO, ^{36}Cl and ^{22}Na in the Mesozoic rocks of northern Switzerland : I. Effective diffusion coefficients and capacity factors across the heterogeneous sediment sequences. Appl. Geochem. 159, 105843. http://dx.doi.org/10.1016/j.apgeochem.2023.105843.

Van Loon, L.R., Soler, J.M., 2003. Diffusion of HTO, $^{36}Cl^-$, $^{125}I^-$ and $^{22}Na^+$ in Opalinus Clay: Effect of Confining Pressure, Sample Orientation, Sample Depth and Temperature. Technical Report TR 03-07, Nagra, Wettingen, Switzerland.

Wersin, P., Mazurek, M., Gimmi, T., 2022. Pore water chemistry of Opalinus Clay revisited: Findings from 25 years of data collection at the Mont Terri Rock Laboratory. Appl. Geochem. 138, 105234. http://dx.doi.org/10.1016/j.apgeochem.2022.105234.

Wigger, C., Van Loon, L.R., 2018. Effect of the pore water composition on the diffusive anion transport in argillaceous, low permeability sedimentary rocks. J. Contam. Hydrol. 213, 40–48. http://dx.doi.org/10.1016/j.jconhyd.2018.05.001.

Williamson, M.A., Rimstidt, J., 1994. The kinetics and electrochemical rate-determining step of aqueous pyrite oxidation. Geochim. Cosmochim. Acta 58, 5443–5454. http://dx.doi.org/10.1016/0016-7037(94)90241-0.

Woolf, L.A., 1975. Tracer diffusion of tritiated water (THO) in ordinary water (H_20) under pressure. J. Chem. Soc. Faraday Trans. 1: Phys. Chem. Condens. Phases 71.

Wu, T., Amayri, S., Drebert, J., Loon, L.R.V., Reich, T., 2009. Neptunium(V) sorption and diffusion in Opalinus Clay. Environ. Sci. Technol. 43, 6567–6571. http://dx.doi.org/10.1021/es9008568.

Zarzycki, P., Lützenkirchen, J., Gilbert, B. (Eds.), 2025. Surface complexation models. Reviews in Mineralogy & Geochemistry, vol. 91A, De Gruyter, Berlin, Germany; Boston, United States of America.